Dissipativity Robustness Enhancement for Dual-Loop Voltage Control of Grid-Forming VSCs

He, Shan; Yang, Zhiqing; Blaabjerg, Frede

Published in:
Proceedings of the IECON 2023- 49th Annual Conference of the IEEE Industrial Electronics Society

DOI (link to publication from Publisher):
10.1109/IECON51785.2023.10311992

Publication date:
2023

Document Version
Accepted author manuscript, peer reviewed version

Dissipativity Robustness Enhancement for Dual-Loop Voltage Control of Grid-FormingVSCs

Shan He
Department of Energy
Aalborg University
Aalborg, Denmark
she@energy.aau.dk

Zhiqing Yang
School of Electrical Engineering and Automation
Hefei University of Technology
Hefei, China
zhiqing.yang@hfut.edu.cn

Frede Blaabjerg
Department of Energy
Aalborg University
Aalborg, Denmark
fbl@energy.aau.dk

***Abstract*—Grid-side current feedforward has proven to be an effective approach in improving the dissipativity of dual-loop voltage control in grid-forming converters. However, due to the control delay, the dissipative characteristic of the converter output impedance can be significantly impacted by the designed resonance frequency of the designed LC-filter and any deviation in the filter parameters. To address this issue, the proposed method in this paper replaces grid-side current feedforward with capacitor current feedforward and capacitor voltage feedforward, resulting in enhanced dissipativity below the Nyquist frequency. Additionally, the proposed method improves the dissipativity robustness against deviation in the LC-filter parameters. Moreover, it allows for the LC-filter resonance frequency to be designed freely, without the need to consider the critical frequency. The effectiveness of this proposed method is validated through a case study.**

***Keywords*—Grid-forming converters, voltage control, dissipation, LC-filter resonance frequency design, LC-filter parameter deviation.**

I. Introduction

With the increasing penetration of distributed energy resources, the demand for grid-forming voltage source converters (VSCs) is becoming more crucial as they have the capability of operating under a weak grid or in islanding mode [1-2]. Nevertheless, the VSC-grid system is subject to significant harmonic stability challenges due to the wide range of variation in grid impedance, and passivity-based impedance shaping recently has attracted lots of attention [3]. Specifically, the real part of the converter output impedance should be non-negative below Nyquist frequency, and the corresponding phase angle will be [-90°, 90°]. Assuming a passive grid impedance, the global small-signal stability of VSC can be secured, even for an interconnected system [4].

The control delay is inevitable in the digital pulse width modulation (PWM) process, usually 1.5 times of sampling period. Moreover, the control delay can jeopardize the dissipativity of converter output impedance, and the non-dissipative region for dual-loop voltage control is between the critical frequency (one-sixth of sampling frequency) and the Nyquist frequency [5]. Grid-side current feedforward (GSCF) is identified as a potential solution to enhance the dissipativity, and the internal stability (i.e., equivalent controlled voltage source in the impedance-based stability analysis) is not affected seen from the point of common coupling (PCC) [6]. However, the LC-filter resonance frequency should be lower than the critical frequency, and the robustness against the parameter deviation is weak since the real part of the converter output impedance is zero with GSCF [7-8].

To overcome the above challenges, this paper proposed a control scheme utilizing capacitor current feedforward (CCF) and capacitor voltage feedforward (CVF). In order to simplify the analysis, the filter capacitance is regarded as a part of grid impedance. Further, the detailed parameter design is given, and the dissipativity robustness is enhanced. Finally, considering the parameter deviation and the different LC-filter resonant frequencies, the GSCF is used for comparison to validate the proposed method.

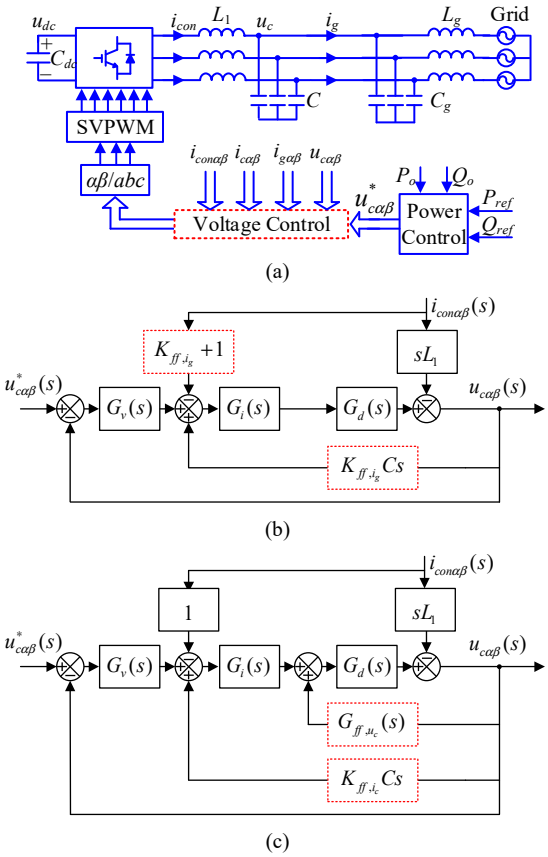

Fig. 1. Dual-loop voltage control diagram of a three-phase grid-forming VSC. (a) Three-phase circuit diagram. (b) With grid-side current feedforward. (c) With capacitor current and capacitor voltage feedforward.

II. Modeling and Dissipativity Analysis Without Grid-Side Current Feedforward

A. System modeling

The investigated dual-loop three-phase grid-forming VSC is depicted in Fig. 1(a), where u_c is the filter capacitor voltage, u_{dc} is the dc-link voltage, i_{con} is the converter-side current, i_c is the filter capacitor current, i_g is the grid-side current, L_1 is the converter-side inductance, C is the filter capacitor. L_g and

C_g are the grid impedance, $u^*_{c\alpha\beta}$ is the voltage reference in the $\alpha\beta$-frame.

Considering C as part of the grid impedance, based on Fig. 1(b), the capacitor voltage is

$$u_{c\alpha\beta}(s) = G_{cl}(s)u^*_{c\alpha\beta}(s) - Z_o(s)i^*_{con\alpha\beta} \quad (1)$$

where $G_{cl}(s)$ is the closed-loop transfer function between the reference voltage and the capacitor voltage, $Z_o(s)$ is the converter output impedance seen from the filter capacitor. Their expressions are given as

$$G_{cl}(s) = \frac{G_v(s)G_i(s)G_d(s)}{1+G_v(s)G_i(s)G_d(s)} \quad (2)$$

$$Z_o(s) = \frac{sL_1 + G_i(s)G_d(s)}{1+G_v(s)G_i(s)G_d(s)}. \quad (3)$$

where $G_v(s)$ and $G_i(s)$ are the voltage controller and the current controller, respectively. $G_d(s)$ is the control delay including 1.5 sampling period T_{sa}, which is given as

$$G_d(s) = e^{-1.5sT_{sa}}. \quad (4)$$

Compared to the proportional-resonant (PR) controller, R controller is selected for the voltage control as it can extend the voltage control bandwidth [5], which is given as

$$G_v(s) = K_{rv}\frac{s\cos\varphi_g - \omega_g\sin\varphi_g}{s^2+\omega_{rc}s+\omega_g^2} \approx \frac{K_{rv}}{s} \quad (5)$$

where ω_g, ω_{rc}, φ_g, and K_{rv} represent the grid fundamental angle frequency, the cut-off angle frequency of the R controller, the compensation angle of the R controller, and the R controller gain, respectively. PR controller is used in the current control, which is given as

$$G_i(s) = K_{pi} + K_{ri}\frac{s\cos\varphi_g - \omega_g\sin\varphi_g}{s^2+\omega_{rc}s+\omega_g^2} \approx K_{pi} \quad (6)$$

where K_{pi} and K_{ri} represent the proportional gain and the R controller gain, respectively. Since the control delay mainly affects the stability in the high-frequency range, the R controller in (5) is simplified as an integrator, and only proportional gain is considered in (6).

According to the passivity theory, a grid-forming VSC can be stabilized if the two constraints are satisfied [3]. First, the closed-loop transfer function $G_{cl}(s)$ should be stable, which can be guaranteed by setting a proper bandwidth. Second, the real part of $Z_o(j\omega)$ is non-negative below Nyquist frequency. In terms of the internal stability design, the open-loop transfer function of the current control is

$$T_{oi}(s) = \frac{G_i(s)G_d(s)}{sL_1} \approx \frac{K_{pi}}{sL_1}e^{-1.5sT_{sa}}. \quad (7)$$

With a given phase margin (PM) φ_m, and the proportional gain of current controller is

$$K_{pi} = \omega_{ci}L_1 = \frac{0.5\pi - \varphi_{mi}}{T_d}L_1. \quad (8)$$

where ω_{ci} is the cut-off angle frequency of open-loop transfer function of current control. Herein, ω_{ci} is set as $\frac{\omega_{sa}}{10}$, and φ_{mi} will be 0.2π, where ω_{sa} is the sampling angle frequency.

Resorting (2), (5) and (6), the open-loop transfer function of voltage control is

$$T_{ov}(s) \approx \frac{K_{rv}K_{pi}}{s}e^{-1.5sT_{sa}}. \quad (9)$$

To decouple the current controller and voltage controller, a lower bandwidth ($\frac{\omega_{sa}}{20}$) is selected. The resonant gain of the voltage controller is

$$K_{rv} = \frac{\omega_{cv}}{K_{pi}}, \quad (10)$$

where ω_{cv} is the cut-off angle frequency of the voltage controller and the PM φ_{mv} is 0.35π.

B. Dissipativity analysis

By Substituting '$s=j\omega$' into (3), the sign of $Re\{Z_o(j\omega)\}$ is

$$\mathrm{sgn}\{\mathrm{Re}\{Z_o(j\omega)\}\} = \mathrm{sgn}\{(-K_{rv}L_1+1)K_{pi}\omega^2\cos(\omega T_d)\}. \quad (11)$$

Based on (11), the dissipative region using dual-loop voltage control is

$$f_{dissipative} = (0, f_{crit}) \quad (12)$$

where the critical frequency is $f_{crit} = 1/4T_d$. The dissipative characteristic of dual-loop voltage control without grid-side current feedforward is shown in Fig. 2, and the deviation of converter-side inductance only affects the amplitude of $Re\{Z_o(j\omega)\}$ but not the dissipative region. The system specifications of the investigated grid-forming VSC are shown in Table I. In this paper, double-sampling control is used, and the Nyquist frequency is 4000 Hz.

When considering the filter capacitance as part of grid impedance, the designed LC-filter resonance frequency should be smaller than the critical frequency to guarantee stability in island operation. As a result, the LC-filter design is limited, and the same conclusion can be acquired through the open-loop internal stability analysis seen from the PCC point [7].

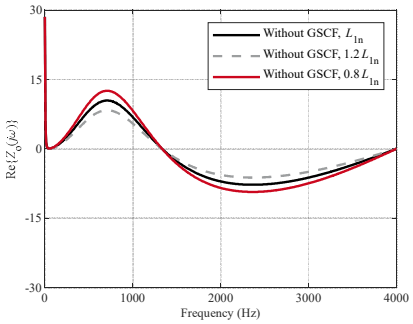

Fig. 2. Dissipative characteristic without grid-side current feedforward.

TABLE I. PARAMETERS OF GRID-FORMING CONVERTER

Symbol	Description	Value	Symbol	Description	Value
P_o	Output power	3.5 kW	u_g	Grid phase voltage (RMS)	110 V
f_{sa}	Sampling frequency	8 kHz	f_{sw}	Switching frequency	4 kHz
L_1	Converter-side inductance	3 mH	C	Filter capacitance	3/15 μF
L_g	Converter-side inductance	3 mH	C_g	Filter capacitance	10 μF

III. DISSIPATIVITY ROBUSTNESS ANALYSIS WITH GRID-SIDE CURRENT FEEDFORWARD

GSCF can effectively enhance the dissipativity of voltage control [5]. Based on Fig. 1(b), the VSC output impedance is

$$Z_o(s)=\frac{sL_1+G_i(s)G_d(s)(1+K_{ff,i_g})}{1+G_i(s)G_d(s)(G_v(s)-sCK_{ff,i_g})}. \quad (13)$$

where K_{ff,i_g} is the GSCF coefficient. By substituting '$s=j\omega$' into (13), the sign of $Re\{Z_o(j\omega)\}$ is

$$\mathrm{sgn}\left\{\mathrm{Re}\left\{Z_o(j\omega)\right\}\right\}=\mathrm{sgn}\left\{\begin{matrix}(-K_{rv}L_1+1\\+K_{ff,i_g}(1-L_1C\omega^2))\\K_{pi}\omega^2\cos(\omega T_d)\end{matrix}\right\}. \quad (14)$$

By changing the sign of $Re\{Z_o(j\omega)\}$ at the critical angle frequency ($2\pi/4T_d$), the proportional GSCF coefficient is

$$K_{ff,i_g}=\frac{K_{rv}L_{1n}-1}{1-L_{1n}C_n\omega_{crit}^2}=\frac{K_{rv}L_{1n}-1}{1-\frac{\omega_{crit}^2}{\omega_{rn}^2}}. \quad (15)$$

where L_{1n} and C_n are the nominal values of converter-side inductance and filter capacitance, ω_{rn} is the nominal resonance frequency. Considering a general case of filter parameter deviations, the dissipative characteristic is shown in Fig. 3. It can be seen that −20% parameter deviation can introduce a larger non-dissipative region than +20% deviation.

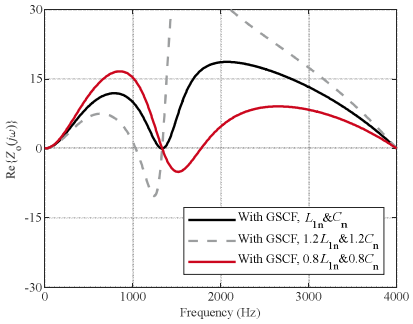

Fig. 3. Dissipative characteristic with grid-side current feedforward when LC-filter resonance frequency is lower than critical frequency (f_{crit}=1333 Hz, f_{rn}=750 Hz).

On the other hand, the designed LC-filter resonance frequency should be smaller than the critical frequency to ensure dissipativity below the Nyquist frequency. Otherwise, there will be no dissipative region, as shown in Fig. 4. Especially, the LC-filter resonance frequency cannot be the same as the critical frequency, because the GSCF coefficient will be infinite according to (15). Further, for island operation with a zero load, K_{ff,i_g} is zero as the load-side current is zero. Then the GSCF cannot contribute to the dissipativity even though $\omega_{rn}<\omega_{crit}$, which is the same as dual-loop control without feedforward.

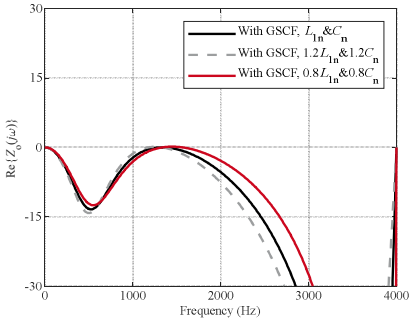

Fig. 4. Dissipative characteristic with grid-side current feedforward when LC-filter resonance frequency is higher than critical frequency (f_{crit}=1333 Hz, f_{rn}=1678 Hz).

IV. Dissipativity Robustness Enhancement

As discussed in Section III, GSCF has two limitations regarding the dissipativity of dual-loop voltage control. First, the LC-filter resonance frequency should be designed lower than the critical frequency. Second, the dissipativity can be easily jeopardized by the LC-filter parameter deviation. To overcome the first limit, the GSFC is replaced by the CCF. To enhance the dissipativity robustness, a moving-average-filter-based capacitor voltage feedforward (CVF) is superimposed. In addition, the CCF coefficient is optimized according to the required LC-filter parameter deviation. It is worth noting that no extra current sensors are needed compared to GSCF, because the sampled capacitor current can be calculated through the bias between the sampled converter-side current and grid-side current. Moreover, converter-side current sensors are mandatory for over-current protection.

A. Capacitor current feedforward

When using CCF, the output impedance is

$$Z_o(s)=\frac{sL_1+G_i(s)G_d(s)}{1+G_i(s)G_d(s)(G_v(s)-sCK_{ff,i_c})}. \quad (16)$$

where K_{ff,i_c} is the CCF coefficient. By substituting '$s=j\omega$' into (16), the sign of $Re\{Z_o(j\omega)\}$ is

$$\mathrm{sgn}\left\{\mathrm{Re}\left\{Z_o(j\omega)\right\}\right\}=\mathrm{sgn}\left\{\begin{matrix}(-K_{rv}L_1+1\\-K_{ff,i_c}L_1C\omega^2)K_{pi}\omega^2\cos(\omega T_d)\end{matrix}\right\}. \quad (17)$$

By changing the sign of $Re\{Z_o(j\omega)\}$ at the critical angle frequency ($2\pi/4T_d$), the CCF coefficient can be derived as

$$K_{ff,i_c}=\frac{1-K_{rv}L_{1n}}{L_{1n}C_n\omega_{crit}^2}. \quad (18)$$

Substituting (18) into (17), the sign of $Re\{Z_o(j\omega)\}$ with CCF is given as

$$\mathrm{sgn}\left\{\mathrm{Re}\left\{Z_o(j\omega)\right\}\right\}=\mathrm{sgn}\left\{\begin{matrix}(1-K_{rv}L_1-\frac{1-K_{rv}L_{1n}}{L_{1n}C_n\omega_{crit}^2}L_1C\omega^2)\\K_{pi}\omega^2\cos(\omega T_d)\end{matrix}\right\}. \quad (19)$$

Consequently, the dissipativity is not limited by the designed LC-filter resonance frequency, even though when the LC-filter resonance frequency is the same as the critical frequency.

As shown in Fig. 5, when the LC-filter resonant frequency is larger than the critical frequency, the dissipativity can be achieved (k=1) compared to Fig. 4. However, the dissipativity is still affected by the LC-filter parameter deviation, and a −20% parameter deviation can introduce a larger non-dissipative region than a +20% deviation.

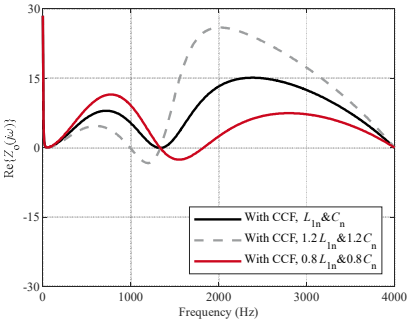

Fig. 5. Dissipative characteristic with capacitor current feedforward considering LC-filter parameter deviations (f_{crit}=1333 Hz, f_{rn}=1678 Hz).

B. Capacitor current feedforward and proportional capacitor voltage feedforward

CVF is commonly used in the current control of grid-following converters to enhance the dissipativity robustness [8], and the converter output impedance is

$$Z_o(s)=\frac{sL_1+G_i(s)G_d(s)}{1+G_i(s)G_d(s)(G_v(s)-sCK_{ff,i_c})-G_{ff,u_c}(s)G_d(s)}. \tag{20}$$

where $G_{ff,u_c}(s)$ is the CVF function. The most direct method is proportional CVF, which is given as

$$G_{ff,u_c}(s)=K_{ff,u_c} \tag{21}$$

By substituting '$s=j\omega$' and (21) into (20), the sign of $Re\{Z_o(j\omega)\}$ considering CCF and proportional CVF is

$$\operatorname{sgn}\left\{\operatorname{Re}\left\{Z_o(j\omega)\right\}\right\}=\operatorname{sgn}\left\{\begin{matrix}(-K_{rv}L_1+1-K_{ff,i_c}L_1C\omega^2)\\ K_{pi}\omega^2\cos(\omega T_d)\\ +(L_1\sin(\omega T_d)\omega-K_{pi})K_{ff,u_c}\omega^2\end{matrix}\right\}. \tag{22}$$

Then the dissipative characteristic of converter output impedance at the critical frequency is

$$\operatorname{sgn}\left\{\operatorname{Re}\left\{Z_o(j\omega_{crit})\right\}\right\}=\operatorname{sgn}\left\{(\omega_{crit}kL_{1n}-K_{pi})K_{ff,u_c}\omega_{crit}{}^2\right\}. \tag{23}$$

Hence, the allowed maximum negative filter parameter deviation is

$$k\geq\frac{K_{pi}}{\omega_{crit}L_{1n}} \tag{24}$$

Recalling (8), the minimum value of k is 0.6 when $K_{pi}=\frac{\omega_{sa}L_{1n}}{10}$. As illustrated in Fig. 6, the dissipativity robustness against the passive filter deviation near the critical frequency can be enhanced with the CVF. However, another non-dissipative region around the Nyquist angle frequency is introduced. The dissipative characteristic at the Nyquist frequency is

$$\operatorname{sgn}\left\{\operatorname{Re}\left\{Z_o(j0.5\omega_{sa})\right\}\right\}=\operatorname{sgn}\left\{\begin{matrix}-(0.5\omega_{sa}kL_{1n}+K_{pi})\\ K_{ff,u_c}\,0.25\omega_{sa}{}^2\end{matrix}\right\}<0. \tag{25}$$

Note that the internal stability should be paid attention especially when adding CVF, and the open-loop transfer function in (9) is modified as

$$T_{ov1}(s)\approx\frac{K_{rv}K_{pi}e^{-1.5sT_{sa}}}{s(1-(K_{ff,i_c}K_{pi}Cs+K_{ff,u_c})e^{-1.5sT_{sa}})}. \tag{26}$$

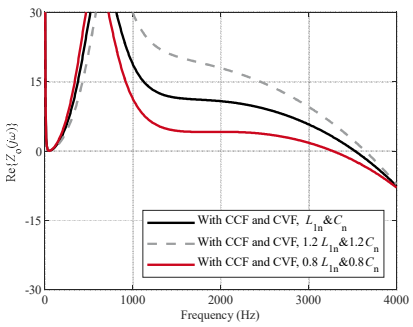

Fig. 6. Dissipative characteristic with capacitor current feedforward and proportional capacitor voltage feedforward (f_{crit}=1333 Hz, f_{rn}=1678 Hz).

Within the voltage control bandwidth, the delay and the derivative terms in (26) can be ignored. Then, (26) is further simplified as

$$T_{o2}(s)\approx\frac{K_{rv}K_{pi}e^{-1.5sT_{sa}}}{s(1-K_{ff,u_c})}. \tag{27}$$

As a result, (10) is modified as

$$K_{rv}=\frac{\omega_{cv}}{K_{pi}}(1-K_{ff,u_c}). \tag{28}$$

The bode diagram of open-loop transfer function with and without simplification is shown in Fig. 7. It can be found that the amplitude-frequency characteristic is almost the same without and with simplification, which validates the effectiveness of (28).

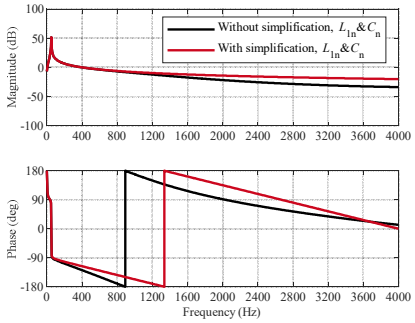

Fig. 7. Bode diagram of open-loop transfer function with and without simplification ($K_{ff,u_c}=0.5$).

C. Capacitor current and moving-average-filter-based capacitor voltage feedforward

When using proportional CVF, the non-dissipative region around the Nyquist frequency is mainly caused by '$\sin(0.5\omega_{sa}1.5T_{sa})$' in (22). To remove this region, an extra $0.5T_{sa}$ delay can be added in the CVF path, i.e., '$\sin(0.5\omega_{sa}2T_{sa})$' becomes zero at the Nyquist frequency. In the practical implementation, a moving average filter (MAF) is used in the CVF path, which is

$$G_{ff,u_c}(s)=K_{ff,u_c}(0.5+0.5e^{-sT_{sa}}). \tag{29}$$

Compared to Fig. 6, the dissipativity around the Nyquist frequency is enhanced, but another non-dissipative region is introduced with a –20% LC-filter parameter deviation (see Fig. 8). Further, a CCF correction term considering negative parameter deviation is added to enhance the dissipativity, which is given as

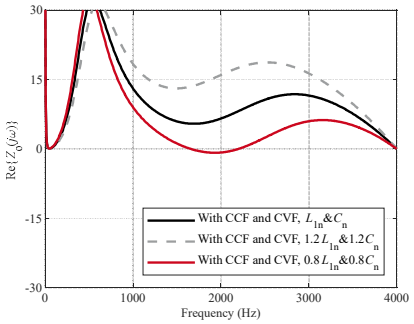

Fig. 8. Dissipative characteristic with capacitor current feedforward and moving-average-filter-based capacitor voltage feedforward (f_{crit}=1333 Hz, f_{rn}=1678 Hz).

$$K_{ff,i_c} = \frac{K_{pi} - K_{rv}K_{pi}L_{1n}m}{L_{1n}C_n m^2 \omega_{crit}^2}. \quad (30)$$

Specifically, m is set to 0.8 considering a −20% parameter deviation. In addition, m can be designed to lower values in terms of the larger parameter deviation. Interestingly, the dissipativity can be still achieved under a +20% parameter deviation when m is 0.8, as shown in Fig. 9.

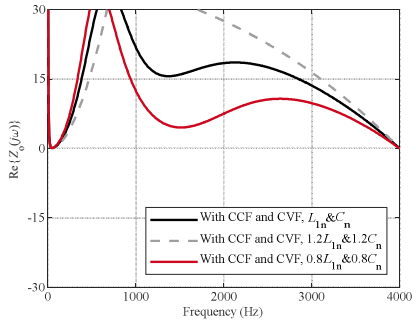

Fig. 9. Dissipative characteristic with corrected capacitor current feedforward and moving-average-filter-based capacitor voltage feedforward. (f_{crit}=1333 Hz, f_{rn}=1678 Hz).

V. Case Study

A. Effect of LC-filter parameter design on dissipativity

To investigate the limitation of LC-filter parameter design on the dissipativity, the LC-filter resonance frequency (1678 Hz) is set as higher than the critical frequency (1333 Hz). Regarding the filter capacitance as part of grid impedance, the equivalent grid impedance is $Z_{g,eq}(s) = \dfrac{sL_g}{1+s^2L_g(C+C_g)}$. It can be seen from Fig. 10 that $Z_o(s)$ intersects with $Z_{g,eq}(s)$ in the negative-real-part region, which leads to a −8.6° PM and destabilizes the system. The related simulation results are given in Fig. 11, where the VSC starts at 20 ms and the power reference is set as zero. It can be seen that only using GSCF cannot stabilize the system and the proposed method can always remain dissipative.

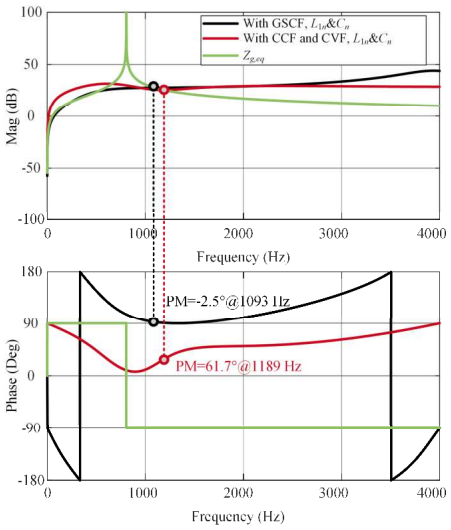

Fig. 10. VSC output impedance $Z_o(s)$ seen from the capacitor (C=15 μF) with L_g=3 mH and C_g=10 μF.

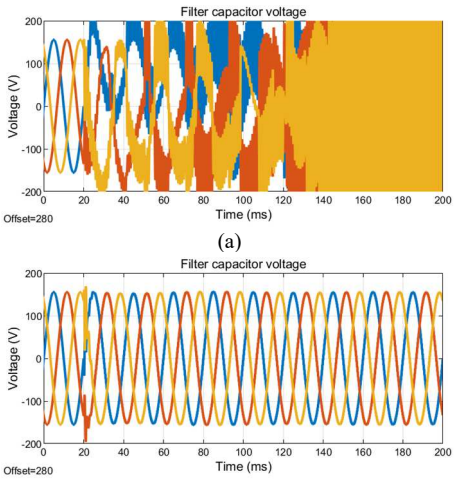

Fig. 11. Dissipativity assessment when LC-filter resonance frequency is lower than critical frequency (f_{rn}=750 Hz, f_{crit}=1333 Hz, L_g=3 mH, C_g=10 μF). (a) With grid-side current feedforward. (b) Proposed method.

B. Effect of LC-filter parameter deviation on dissipativity

Even though the LC-filter resonance frequency (750 Hz) is higher than the critical frequency (1333 Hz), the dissipativity around the critical frequency is weak with GSCF. Considering a −20% deviation of nominal values of L_1 and C, as shown in Fig. 12, the system still cannot be stabilized for the GSCF (PM=−36.3°). After implementing the proposed method, the system becomes stable and the PM is 4.4°, as shown in Fig. 13.

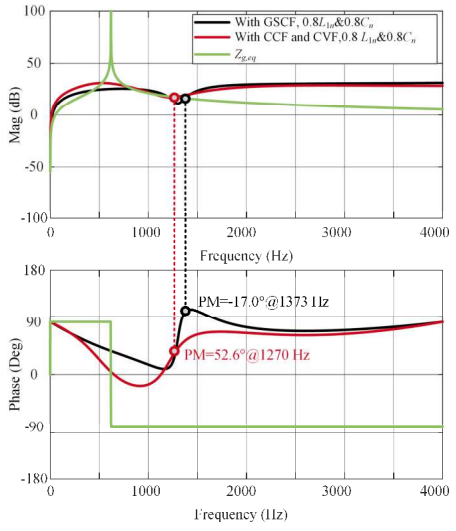

Fig. 12. VSC output impedance $Z_o(s)$ seen from the capacitor (C=3 μF) with L_g=3 mH and C_g=10 μF.

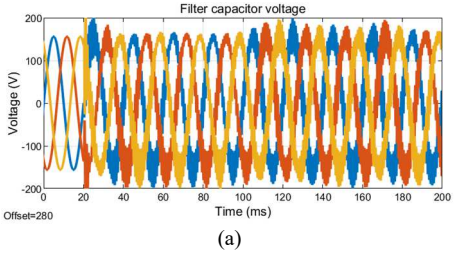

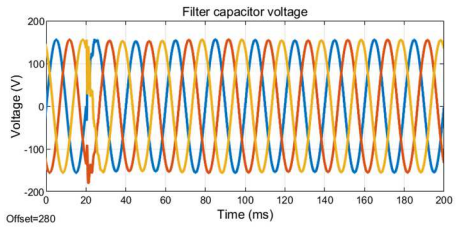

(b)

Fig. 13. Simulation results with a −20% deviation of L_1 and C (f_m=1678 Hz, f_{crit}=1333 Hz, L_g=3 mH, C_g=10 μF). (a) With grid-side current feedforward. (b) Proposed method.

VI. Conclusion

This paper first investigates the dissipativity for dual-loop voltage control of grid-forming VSCs. It is pointed out that the LC-filter resonance frequency should be designed lower than the critical frequency, for the cases with/without grid-side current feedforward. Further, the dissipativity around the critical frequency is vulnerable in terms of LC-filter parameter deviation for grid-side current feedforward. To tackle the challenge of the LC-filter design, the grid-side current feedforward is replaced by the capacitor current feedforward. To enhance the dissipativity robustness against parameter deviation, a correction term is added in the capacitor current feedforward. In addition, a moving-average-filter-based capacitor voltage feedforward is superimposed. As a result, the dissipative region is optimized to Nyquist frequency, and the dissipativity robustness is enhanced at the same time. Finally, the proposed method is validated through the case study.

Acknowledgment

This work was supported by Reliable Power Electronics Based Power System Project at the Department of Energy, Aalborg University, as a part of the Villum Investigator Program funded by the Villum Foundation.

References

[1] R. H. Lasseter, Z. Chen, and D. Pattabiraman, "Grid-forming inverters: A critical asset for the power grid," *IEEE J. Emerg. Sel. Top. Power Electron.*, vol. 8, no. 2, pp. 925–935, Jun. 2020.

[2] R. Rosso, X. Wang, M. Liserre, X. Lu, and S. Engelken, ''Grid-forming converters: control approaches, grid-synchronization, and future trends—A review,'' *IEEE Open J. Ind. Appl.*, vol. 2, pp. 93–109, 2021.

[3] L. Harnefors, X. Wang, A. Yepes, and F. Blaabjerg, "Passivity-based stability assessment of grid-connected VSCs-An overview," *IEEE J. Emerg. Sel. Top. Power Electron.*, vol. 4, no. 1, pp. 116–125, Mar. 2016.

[4] L. Harnefors, A. Yepes, A. Vidal, and J. Doval-Gandoy, "Passivity-based controller design of grid-connected VSCs for prevention of electrical resonance instability," *IEEE Trans. Ind. Electron.*, vol. 62, no. 2, pp. 702–710, Feb. 2015.

[5] Y. Liao, X. Wang, and F. Blaabjerg, "Passivity-based analysis and design of linear voltage controllers for voltage-source converters," *IEEE Open J. Ind. Electron. Soc.*, vol. 1, pp. 114–126, June 2020.

[6] G. Wu, Y. He, H. Zhang, X. Wang, D. Pan, X. Ruan, and C. Yao, "Passivity-based stability analysis and generic controller design for grid-forming inverter," *IEEE Trans. Power Electron.*, *early access*, 2023.

[7] A. Akhavan, S. Golestan, J. Vasquez, and J. Guerrero, "Passivity enhancement of voltage-controlled inverters in grid-connected microgrids considering negative aspects of control delay and grid impedance variations," *IEEE J. Emerg. Sel. Topics Power Electron.*, vol. 9, no. 6, pp. 6637–6649, Dec. 2021.

[8] X. Wang, P. C. Loh, and F. Blaabjerg, "Stability analysis and controller synthesis for single-loop voltage-controlled VSIs," *IEEE Trans. Power Electron.*, vol. 32, no. 9, pp. 7394–7404, Sep. 2017.

[9] C. Xie, K. Li, J. Zou, and J. Guerrero, "Passivity-based stabilization of LCL-type grid-connected inverters via a general admittance model," *IEEE Trans. Power Electron.*, vol. 35, no. 6, pp. 6636-6648.